





Cite this: *Phys. Chem. Chem. Phys.*,
2019, 21, 2843

Density-based descriptors and exciton analyses for visualizing and understanding the electronic structure of excited states†

Stefanie A. Mewes *^{ab} and Andreas Dreuw *^a

Analysis and interpretation of the electronic structure of excited electronic states are prerequisites for developing a fundamental understanding of photochemistry and optical properties of molecular systems and an everyday task for a computational photochemist. Hence, wavefunction-based and density-based analysis tools have been devised over the last decades, and most recently also a family of quantitative exciton-wavefunction based descriptors has been developed. While the latter represent the main focus of this perspective, they are also discussed in the context of other existing analysis methods. Exciton analysis bridges the gap between the physically intuitive exciton picture and complex quantum-chemical wavefunctions by yielding insightful quantitative descriptors like exciton size, hole and electron size, electron–hole distance and exciton correlation. Thereby, not only a comprehensive characterization of the electronic structure is provided, but moreover, the formalism is automatizable and thus also optimally suited for benchmarking excited-state electronic structure methods.

Received 21st November 2018,
Accepted 20th January 2019

DOI: 10.1039/c8cp07191h

rscl.li/pccp

^a Interdisciplinary Center for Scientific Computing, Im Neuenheimer Feld 205 A, 69120 Heidelberg, Germany. E-mail: dreuw@uni-heidelberg.de; Tel: +49 6211 5414735

^b New Zealand Institute for Advanced Studies (NZIAS) and Centre for Theoretical Chemistry and Physics (CTCP), Massey University Albany, Private Bag 102904, Auckland 0632, New Zealand

† Electronic supplementary information (ESI) available: Electron–hole correlation plots for first five singlet excited states of *para*-nitrodimethylaniline. Definitions of excited-state descriptors of Etienne *et al.* and Maschietto *et al.* Raw data of Fig. 4, 7, 8 and 11. All optimized molecular geometries. See DOI: 10.1039/c8cp07191h

1 Introduction

Over the last decades, the scope of quantum-chemical excited-state methods has substantially grown and it is nowadays possible to compute excited states of ever larger and more complex molecules.^{1–3} However, with increasing complexity of the molecular or electronic structure also the interpretation of the results of such computations becomes ever more difficult. Therefore it is necessary to extract relevant properties of the excited states,



Stefanie A. Mewes

Stefanie Mewes studied Chemistry at Heidelberg University. She received her PhD in the group of Andreas Dreuw at the Interdisciplinary Center for Scientific Computing in 2018, where she worked on the development of exciton analysis tools. In 2016 she became an honorary fellow of the New Zealand Institute for Advanced Studies, Massey University Auckland, where she is currently working as a postdoc mentored by Prof. Peter Schwerdtfeger. Her

research interests are the development of analysis tools for excited states and excited-state methods and their application in photochemistry.



Andreas Dreuw

Andreas Dreuw received his PhD in theoretical chemistry from Heidelberg University in 2001. After a two-year postdoc at the University of California Berkeley, he joined the Goethe University of Frankfurt first as an Emmy-Noether fellow and then as a Heisenberg Professor for Theoretical Chemistry. Since 2011, Andreas Dreuw has held the chair for Theoretical and Computational Chemistry at the Interdisciplinary Center for Scientific Computing,

Heidelberg University. His research interests comprise the development of electronic structure methods and their application in photochemistry, mechanochemistry, biophysics, and materials science.

which characterize their electronic structure quantitatively to gain detailed insight into optical properties and to achieve a fundamental understanding of light-induced molecular processes in large systems. In chemistry, the standard approach to analyze quantum-chemical calculations and to relate their results to experimental findings is the visual inspection of molecular orbitals (MOs). This approach had and still has great success for electronic ground states when one-particle theories like Hartree-Fock, density functional theory or semi-empirical MO theories are the underlying methods. Great concepts guiding synthesis and interpretation of experimental findings could thereby be derived.⁴ However, for the interpretation of correlated excited-state theories and complex electronic structures this approach has clear limitations.

In advanced excited-state methods, like equation-of-motion (EOM) or linear response (LR) coupled-cluster (CC) methods,^{5–9} or algebraic diagrammatic construction (ADC) schemes for the polarization propagator,^{10–12} for example, the transition vector does not describe the transition from one orbital to another in an excited Slater-determinant, but instead a one-particle excitation from one correlated state to another. In these theories, the excited-state many-body wavefunctions are for instance parametrized as

$$|\Psi_I\rangle = \left\{ \sum_{ia} x_{ia} \hat{a}_a^\dagger \hat{a}_i + \sum_{ia,jb} x_{ia,jb} \hat{a}_a^\dagger \hat{a}_i \hat{a}_b^\dagger \hat{a}_j \dots \right\} |\Psi_{0,\text{corr}}\rangle, \quad (1)$$

with $|\Psi_{0,\text{corr}}\rangle$ being the correlated, many-body electronic ground state wavefunction, \hat{a}_a^\dagger and \hat{a}_i the creation and annihilation operators of second quantization, and the indices $i, j \dots$ and $a, b \dots$ refer to occupied and unoccupied one-particle states of the electronic ground state, respectively. An interpretation of the transition amplitudes $x_{ia}, x_{ia,jb} \dots$ based on MOs does not provide a complete and clear picture, as it corresponds only to a zeroth-order interpretation and thus captures just the uncorrelated part of the story. In predominantly one-electron transitions, *i.e.*, singly excited states, and when essentially only one occupied i and one virtual orbital a contribute with a large transition amplitude x_{ia} an interpretation of the electronic structure in terms of these MOs alone is indeed useful and insightful. This has led for example to the typical classifications of excited states as $\pi\pi^*$, $n\pi^*$, $\sigma\sigma^*$ *etc.* just referring to the main orbital transition. This situation changes, however, as soon as several different orbital transitions contribute to the excited wavefunction, for example when the MOs optimized for the electronic ground state are not suitable for the excited state. In particular when singly, doubly and even higher excited configurations start mixing and when the electron correlation changes strongly in the excited states, then an MO based interpretation is no longer meaningful and the real many-body wavefunction $|\Psi_I\rangle$ needs to be analyzed.

A direct analysis of the many-body excited-state wavefunction of eqn (1), for example by direct visualization or plotting is, however, also only of little help due to its high-dimensional nature and its inherently complicated structure. Hence, since a long time researchers are looking for suitable ways to understand

and interpret the electronic structure of excited states. Historically, excited states are typically classified by the changes in electronic structure occurring upon excitation. Following this line of thought, a naturally occurring quantity for the analysis of complicated electronic structures is the one-particle electron density $\rho(r)$. It is not only a three-dimensional quantity, and as such directly and easy to visualize, but moreover a real physical observable. For example, upon contraction with the dipole moment operator it provides the dipole matrix elements determining the transition probability and is thus experimentally accessible. For the analysis of excited states, it is thus apparent to study their electronic structure as difference between the electron densities of ground and excited state as so-called one-electron difference density

$$\rho_{\Delta}^{\text{of}}(r) = \rho^I(r) - \rho^0(r), \quad (2)$$

which in the MO representation corresponds to the one-electron difference density matrix (1DDM). Not surprisingly, excited-state analysis tools and simple descriptors have been developed based on the 1DDM, which will be analyzed in the course of this article.

A second important quantity for the analysis of excited-state electronic structures is the one-electron transition density

$$\rho_{\text{T}}^{\text{of}}(r_1) = \int \dots \int \Psi_0(r_1, r_2, \dots, r_N) \Psi_I(r_1, r_2, \dots, r_N) dr_2 \dots dr_N. \quad (3)$$

As the name expresses, this density does not directly characterize the electronic structure of the electronic state but more-over the nature of the electronic transition. In other words, the transition density describes the dynamical changes, *i.e.*, the induced oscillations of the ground-state electron density by the absorption of a photon. Hence it characterizes the vertical nature of the electronic transition. The one-electron transition density $\rho_{\text{T}}^{\text{of}}(r)$ and its MO representation, the one-electron transition density matrix (1TDM) serve as starting point for several excited-state analysis tools,^{13–15} some of which will be introduced in detail later and compared to 1DDM-based methods.

One major focus of this article will, however, lie on a newly developed exciton analysis, which bridges the gap between the physically intuitive exciton quasi-particle picture and complicated excited-state wavefunctions originating from quantum-chemical calculations. As will be seen below, these exciton analysis tools rely on the relation of the transition density to the two-particle exciton wavefunction, which makes a straightforward calculation of expectation values and exciton properties possible giving access to easily interpretable quantities. Exciton analysis serves not only for excited-state analysis, but has turned out to be extremely useful for standardized benchmarking of approximate quantum-chemical methods. In the following, different, independently developed excited-state descriptors will be compared and discussed in context, for the first time. Most of them were initially designed as measure for the amount of charge-transfer (CT) character serving as diagnostic tools for the applicability of standard linear-response time-dependent density functional theory (TDDFT).^{1,16,17}

2 Excitons in molecular quantum chemistry

The exciton picture originates from solid-state physics and an exciton is typically generated by absorption of a photon and seen as the quasi-particle consisting of the created positive electron-hole and the excited electron. Both are coupled to each other most dominantly by classical Coulomb attraction, but also by exchange repulsion and correlation effects.^{18–20} Excitons are typically used to describe the character of excited electronic states as Wannier (delocalized), Frenkel (localized) or charge-transfer excitons.^{21,22} By transferring the concept of excitons from extended to molecular systems, and hence extracting exciton properties from quantum chemically obtained quantities, it becomes possible to gain genuine insight into the excited-state electronic structure also of finite, even small molecules.

The central idea of our approach²³ is the identification of an exciton wavefunction as one-particle transition density matrix (1TDM) between the ground (Ψ_0) and an excited (Ψ_I) state and the recognition of the ground-state part as hole coordinate, while the excited-state part represents the electron coordinate leading to

$$\chi_{\text{exc}}(r_h, r_e) = \int \cdots \int \Psi_0(r_h, r_2, \dots, r_N) \Psi_I(r_e, r_2, \dots, r_N) dr_2 \dots dr_N, \quad (4)$$

where N is the number of electrons and r_i are the spatial-spin coordinates. The two-particle wavefunction $\chi_{\text{exc}}(r_h, r_e)$ can be used like any quantum-mechanical wavefunction to compute expectation values, *i.e.*, exciton properties or so-called exciton descriptors, which offer new ways of interpreting molecular

excited-state electronic structure. While the 1TDM itself can also be used to analyze one-electron transition properties as described above, in the following, the focus will lie on properties related to the exciton picture.

When determining the character of an excited state, a central property of interest is the amount of charge transfer occurring between different fragments of a molecular system. This information can be crucial, in particular in the context of TDDFT, to select an appropriate computational protocol or a suitable exchange–correlation (xc-) functional. For this purpose, two different excited-state descriptors have been designed, which are capable of detecting different types of charge transfer: (1) CT accompanied with a permanent shift of electron density and a resulting static dipole moment, and (2) charge-resonance-type CT, *i.e.*, no net charge transfer occurs. For the first type of CT, it is sufficient to measure the distance between the hole and the electron of the exciton characterized as two oppositely charged centroids, *cf.* Fig. 1(a).²⁴ The positions of these centroids \tilde{x}_e and \tilde{x}_h are given as expectation values of the exciton wavefunction of the position operator \hat{x} and their distance is simply calculated according to

$$d_{h \rightarrow e} = |\langle \tilde{x}_e - \tilde{x}_h \rangle_{\text{exc}}| \quad (5)$$

$$= |\langle \tilde{x}_e \rangle_{\text{exc}} - \langle \tilde{x}_h \rangle_{\text{exc}}|. \quad (6)$$

However, it is generally advisable to refer to the so-called exciton size, which takes both the distance between the charge centroids and the spatial extension of the electron and hole clouds into account, and which also considers electron-hole correlation. In that way, it is possible to detect so-called hidden charge transfer²⁵ or charge resonance, and the formation of bound or repulsive excitons,²⁶ *cf.* Fig. 1(c)–(e). This quantity is

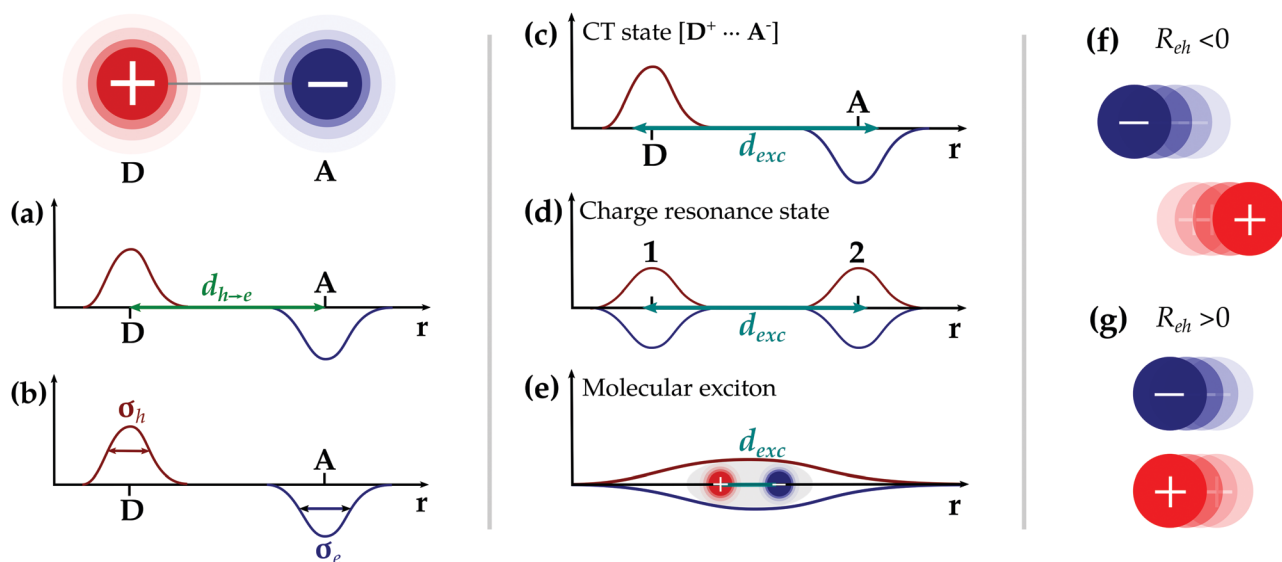


Fig. 1 Exciton descriptors. (left) Exciton properties of a charge-transfer excited state, where charge is promoted from donor **D** to acceptor **A**: (a) distance between electron and hole centroids $d_{h \rightarrow e}$, (b) hole and electron sizes, σ_h and σ_e , describe the root-mean-square distribution of hole and electron around their centres of masses. (middle) Exciton size: three example cases: (c) charge-transfer state [**D**⁺...**A**[−]], (d) charge resonance state between two monomers [**1**⁺...**2**⁺] + [**1**[−]...**2**[−]], (e) molecular exciton in quasi one-dimensional π -conjugated molecule. (right) Electron–hole correlation: (f) electron and hole effectively repel each other, (g) electron and hole move together as expected for exciton binding.

defined as root-mean-square (rms) separation between the instantaneous electron and hole positions

$$d_{\text{exc}} = \sqrt{\langle |\vec{x}_{\text{h}} - \vec{x}_{\text{e}}|^2 \rangle_{\text{exc}}} \quad (7)$$

For measuring the spatial extension of electron and hole densities around their centers-of-charges, *cf.* Fig. 1(b), their variances are evaluated as

$$\sigma_{\text{h}} = \sqrt{\langle \vec{x}_{\text{h}}^2 \rangle_{\text{exc}} - \langle \vec{x}_{\text{h}} \rangle_{\text{exc}}^2} \quad (8)$$

or

$$\sigma_{\text{e}} = \sqrt{\langle \vec{x}_{\text{e}}^2 \rangle_{\text{exc}} - \langle \vec{x}_{\text{e}} \rangle_{\text{exc}}^2} \quad (9)$$

This information is especially valuable when excited states involve special types of electronic transitions, for example, core-excited²⁷ or Rydberg states,²⁸ in which hole and electron densities generally possess very different spatial sizes.

An even further advanced class of descriptors is designed to characterize electron–hole correlation, *i.e.*, the interdependent spatial distribution of electron and hole. The first so-called statistical descriptor is the covariance between the joint electron and hole positions defined as

$$\text{COV}(r_{\text{h}}, r_{\text{e}}) = \langle \vec{x}_{\text{h}} \cdot \vec{x}_{\text{e}} \rangle_{\text{exc}} - \langle \vec{x}_{\text{h}} \rangle_{\text{exc}} \cdot \langle \vec{x}_{\text{e}} \rangle_{\text{exc}} \quad (10)$$

Negative values in COV indicate the electron and hole quasiparticles to dynamically avoid or repel each other in space due to exchange repulsion or correlation effects, see Fig. 1(f). A value of zero indicates no linear electron–hole correlation, which is usually assumed when MOs are analyzed, since MOs provide only the probability of finding the electron or hole somewhere in the molecule independent of its actual motions and independent of all other particles. Positive values in COV on the contrary hint towards the formation of bound excitons, *i.e.*, a joint motion of the electron–hole pair in space due to their electrostatic interaction, *cf.* Fig. 1(g). The value range of COV depends on the electron and hole sizes, which makes a comparison meaningful only for excited states belonging to the same system. To compare the “pure” electron–hole correlation it is advisable to use the normalized electron–hole correlation coefficient defined as

$$R_{\text{eh}} = \frac{\text{COV}(r_{\text{h}}, r_{\text{e}})}{\sigma_{\text{h}} \sigma_{\text{e}}} \quad (11)$$

R_{eh} is thus the normed covariance with respect to the electron and hole sizes. Its values range between $\{-1, \dots, 0, \dots, +1\}$ and their interpretation is fully analogous to the previous one of COV. Due to the better comparability, R_{eh} is usually the measure of choice to analyze electron–hole correlation effects in molecular systems.

The presented exciton analysis can be combined with any excited-state method which provides access to the 1TDM. So far, it has been combined with a wide range of methods, namely, equation-of-motion coupled cluster,²⁸ the algebraic-diagrammatic construction of the polarization propagator methods (ADC n family),²³ time-dependent density functional theory (TDDFT and TDA),²⁹ configuration interaction singles,

and the GW+Bethe–Salpeter method,³⁰ as well as the complete-active-space self-consistent field method (CASSCF) and its perturbation-theory variant CASPT2.³¹

3 Characterization of excited electronic states

Determining the character of electronic transitions is important in quantum-chemical investigations of excited states to gain insight into the electronic structure and to arrive at structure–property relationships which allow for a basic understanding of photochemistry and optical properties of molecular systems. The excited-state character, *i.e.*, whether it is an $n\pi^*$, $\pi\pi^*$, CT state *etc.*, is directly connected to the excited-state properties and usually allows for predictions of *e.g.* the interaction with an environment, reaction pathways, de-excitation processes, *etc.*

A common strategy for determining the excitation character is to analyse the molecular orbitals (MOs) contributing to the excitation vector as has been described in the Introduction. Since ground state MOs are however not necessarily the best choice to represent the excitation process, an alternative orbital representation, specifically designed for the description of electronic transition, are the so-called natural transition orbitals (NTOs).^{13,32–34} These are obtained by a singular value decomposition of the one-particle transition density matrix and provide a compact, state-specific description of the electronic transition, such that couplings between excited electron and electron–hole are explicitly considered. Natural transition orbitals have predictive power even beyond ordinary single excitation processes and can *e.g.* provide insight into two-photon absorption processes³⁵ and meta-stable excited states.³⁶ As we have seen in the previous section, the exciton properties are inherently connected to the 1TDM and in turn to the NTO picture,²⁴ and along this line of thought, exciton descriptors can also be determined for perturbed 1TDMs providing insight into non-linear processes,³⁵ and for meta-stable states, in which the real and imaginary parts of the resonance wave functions are analyzed separately.³⁶ Another orbital representation is given by natural difference orbitals (NDO),³⁸ which are those orbitals that diagonalize the one-electron difference density matrix (1DDM). In contrast to NTOs, which characterize the vertical electronic transition, NDOs take orbital relaxation of the excited state into account. However, though generally useful, NDOs are not frequently employed, but instead detachment/attachment density plots³⁴ are more prominent, which are also derived from the 1DDM. For that objective the 1DDM is diagonalized and split into those matrices which contain the negative (detachment) eigenvalues and positive (attachment) eigenvalues. The detachment density thus corresponds to that part of the density that is removed upon excitation and rearranged as attachment density. Together, these densities fully determine the character of the excited electronic state. Visualization of NTOs, NDOs, transition or difference densities as well as plotting detachment and attachment densities are highly useful in identifying the excited-state character, *i.e.*, its electronic structure, and to relate

it to observed properties. The main disadvantage in this context is, however, that they do not offer a quantitative description of the excitation process or the electronic structure of excited states, but rely on visual interpretation by the beholder. The exciton analysis and the derived descriptors introduced in the previous section, on the other hand, provide a quantitative analysis independent of the eye of the beholder. Another important aspect of this quantitative excited-state analysis is that it allows for thorough and quantitative comparison of different computational protocols,²⁸ and thus opens new possibilities for benchmarking excited-state methods, as will be described in more detail below.

To illustrate further how excited states can be characterized using exciton properties, let us consider a model dimer and its expectation values for eight excitation patterns (Fig. 2) along a molecular separation d .^{23,37} A fully symmetric dimer is chosen on purpose, since its degenerate excited states are very difficult to characterize in general by inspection of molecular orbitals or densities. Generally, the excited states are categorized into four groups, and localized as well as delocalized states are considered. In the case of localized states, each monomer can be excited individually leading to two locally excited states $|1^* 2\rangle$ and $|1 2^*\rangle$, or an electron can be promoted from one monomer to the other yielding two charge-transfer states $|1^+ 2^-\rangle$ and $|1^- 2^+\rangle$. For delocalized states, negative and positive linear combinations can be constructed from the locally excited states leading to excitonic resonance states σ and γ , and from the charge-transfer states yielding two charge resonance states δ and ρ . If we furthermore consider the initial orbitals to have root-mean-square sizes of $\sigma_{h,1}$ and $\sigma_{h,2}$ and the final orbitals to have sizes of $\sigma_{e,1}$ and $\sigma_{e,2}$, we obtain a set of expectation values for the exciton descriptors as summarized in Tables 1 and 2. In general, the transformation from localized to delocalized states is a unitary transformation of the molecular orbitals and states.

The exciton size is evaluated with respect to the other descriptors by using the relationship

$$d_{\text{exc}} = \sqrt{d_{h \rightarrow e}^2 + \sigma_h^2 + \sigma_e^2 - 2\text{COV}}. \quad (12)$$

In the case of localized excited states (*cf.* Table 1), the hole and electron sizes simply reflect on which fragment 1 or 2 the

created hole or excited electron are located. In an asymmetric excitonically coupled system, these numbers would reflect the size of the respective orbitals involved. Furthermore, the descriptor $d_{h \rightarrow e}$ distinguishes between locally excited states, for which it is zero, and charge-transfer states. In the latter case, it corresponds to the spatial separation of 1 and 2, *i.e.*, d . All of these quantities directly enter into the exciton size, *cf.* eqn (12). To evaluate the covariance, we calculate mixed dipole moments between initial and final orbitals. For more details, the reader is referred to ref. 23.

In general, some principle relations between different descriptors can be proposed when determining the character of an excited state. For example, in the case of a Rydberg state, the electron size needs to be significantly larger than the hole size, $\sigma_e > \sigma_h$. For permanent CT states, the charge centroid distance is expected to be significant $d_{h \rightarrow e} > 0$. For bound molecular excitons, electron-hole correlation is expected to be significantly positive $R_{eh} > 0$. For core-excited states, the hole size is expected to be very small $\sigma_h \ll 1 \text{ \AA}$.

Categorizing excited states in terms of exciton properties has the additional advantage over inspecting visualization approaches that it can be automatized. This is particularly attractive for data-driven investigations where the task is to optimize a class of compounds and to finetune its excited-state properties to match design goals. Hirose *et al.*³⁰ proposed a scheme for this purpose by combining the ratio of $d_{h \rightarrow e}/d_{\text{exc}}$ and the orbital overlap A ³⁹ to differentiate between five types of excited states. In that manner, several key properties can be identified and finetuned to obtain an optimal molecular design for a specific purpose. While the authors show this classification scheme not to be ideal, it can be seen as a starting point for developing a more predictive scheme.

As a second example, the first five singlet excited states of *para*-nitrodimethylaniline^{41,42} have been calculated at ADC(2)/6-311G(d,p)⁴⁰ level and are characterized in Table 3 and visualized in terms of electron and hole densities in Fig. 3. The first excited state $1^1A''$ has a $n\pi^*$ excitation character localized on the nitro group. This state has a small charge-transfer character with $d_{h \rightarrow e} = 0.71 \text{ \AA}$ and respectively small hole and electron sizes ($\sigma_h = 1.4 \text{ \AA}$ and $\sigma_e = 1.85 \text{ \AA}$). The second excited state $2^1A'$ is a charge-transfer state, where the charge is promoted from the NMe_2 towards NO_2 , where both, the hole and electron density are delocalized also over the phenyl ring. The distance between hole and electron centroids is as large as 2.31 \AA and both, hole and electron sizes are significantly larger than in the previous case with 2.39 \AA and 2.50 \AA , respectively. As opposed to the previous state, this state shows significant electron-hole correlation with $R_{eh} = 0.103$. The third excited state is the $3^1A'$ state, which can be characterized by a transition of electron density from NMe_2 and the phenyl π -system into a pure π^* orbital located at the phenyl ring. This state possesses only a small CT character and insignificant electron-hole correlation. However, the large hole size of 2.29 \AA gives rise to a larger exciton size as compared to the S_1 . The fourth excited state $2^1A''$ is again characterized by a $n\pi^*$ transition located on the nitro group and has very similar properties as compared to the S_1 . The fifth excited

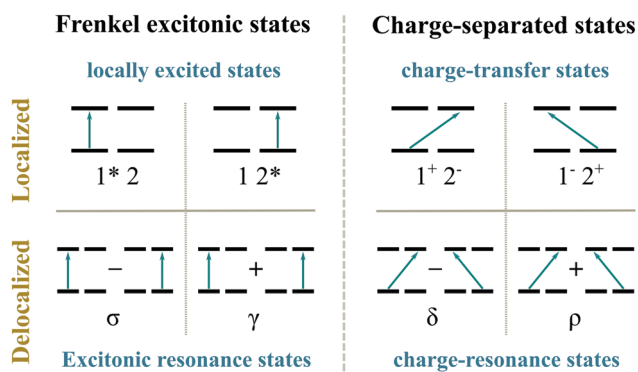


Fig. 2 Excited states of a model dimer with one occupied and one unoccupied orbital at each monomer site. Adopted from ref. 37.

Table 1 Expectation values of exciton descriptors for localized excited states of a model dimer

	$ 1^* 2\rangle$	$ 1 2^*\rangle$	$ 1^+ 2^-\rangle$	$ 1^- 2^+\rangle$
d_{exc}	$\sqrt{\sigma_{\text{h},1}^2 + \sigma_{\text{e},1}^2 - 2\text{COV}}$	$\sqrt{\sigma_{\text{h},2}^2 + \sigma_{\text{e},2}^2 - 2\text{COV}}$	$\sqrt{d^2 + \sigma_{\text{h},1}^2 + \sigma_{\text{e},2}^2 - 2\text{COV}}$	$\sqrt{d^2 + \sigma_{\text{h},2}^2 + \sigma_{\text{e},1}^2 - 2\text{COV}}$
σ_{h}	$\sigma_{\text{h},1}$	$\sigma_{\text{h},2}$	$\sigma_{\text{h},1}$	$\sigma_{\text{h},2}$
σ_{e}	$\sigma_{\text{e},1}$	$\sigma_{\text{e},2}$	$\sigma_{\text{e},2}$	$\sigma_{\text{e},1}$
$d_{\text{h} \rightarrow \text{e}}$	0	0	d	d
COV	$M_{ii}^{(1)} M_{jj}^{(1)}$	$M_{ii'}^{(1)} M_{jj'}^{(1)}$	$M_{ii}^{(1)} M_{jj'}^{(1)}$	$M_{ii'}^{(1)} M_{jj}^{(1)}$

Table 2 Expectation values of exciton descriptors for delocalized excited states of a model dimer

	σ	γ	δ	ρ
d_{exc}	$\sqrt{\frac{1}{4}[(\sigma_{\text{h},1} + \sigma_{\text{h},2})^2 + (\sigma_{\text{e},1} + \sigma_{\text{e},2})^2] - 2\text{COV}}$		$\sqrt{d^2 + \frac{1}{4}[(\sigma_{\text{h},1} + \sigma_{\text{h},2})^2 + (\sigma_{\text{e},1} + \sigma_{\text{e},2})^2] - 2\text{COV}}$	
σ_{h}	$\frac{1}{2}(\sigma_{\text{h},1} + \sigma_{\text{h},2})$	$\frac{1}{2}(\sigma_{\text{h},1} + \sigma_{\text{h},2})$	$\frac{1}{2}(\sigma_{\text{h},1} + \sigma_{\text{h},2})$	$\frac{1}{2}(\sigma_{\text{h},1} + \sigma_{\text{h},2})$
σ_{e}	$\frac{1}{2}(\sigma_{\text{e},1} + \sigma_{\text{e},2})$	$\frac{1}{2}(\sigma_{\text{e},1} + \sigma_{\text{e},2})$	$\frac{1}{2}(\sigma_{\text{e},1} + \sigma_{\text{e},2})$	$\frac{1}{2}(\sigma_{\text{e},1} + \sigma_{\text{e},2})$
$d_{\text{h} \rightarrow \text{e}}$	0	0	d	d
2-COV	$M_{ii}^{(1)} M_{jj}^{(1)} + M_{ii'}^{(1)} M_{jj'}^{(1)} - 2M_{ii'}^{(1)} M_{jj}^{(1)}$		$M_{ii}^{(1)} M_{jj'}^{(1)} + M_{jj}^{(1)} M_{ii'}^{(1)} + 2M_{ii'}^{(1)} M_{jj}^{(1)}$	

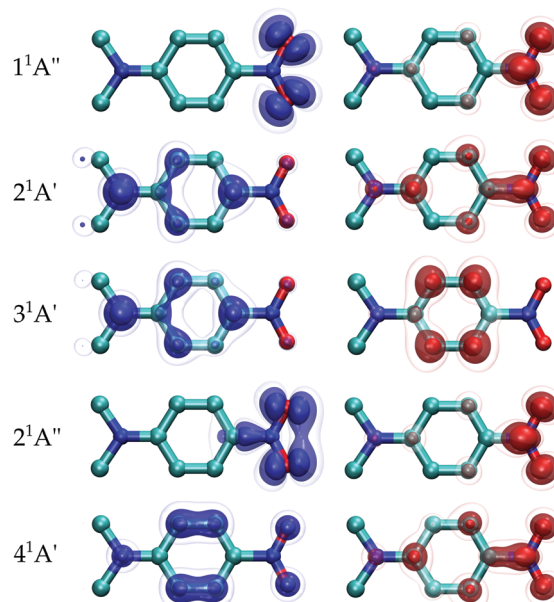
Table 3 Characterization of the first five singlet excited states of *para*-nitrodimethylaniline calculated at the ADC(2)/6-311G(d,p)⁴⁰ level of theory in terms of symmetry label, excitation energy (ΔE , eV), oscillator strength (f_{osc}), exciton size (d_{exc} , Å), charge centroid distance ($d_{\text{h} \rightarrow \text{e}}$, Å), hole and electron sizes (σ_{h} and σ_{e} , Å), electron–hole correlation coefficient (R_{eh}) and transition type

State	ΔE	f_{osc}	d_{exc}	$d_{\text{h} \rightarrow \text{e}}$	σ_{h}	σ_{e}	R_{eh}	Type
$1^1\text{A}''$	3.89	0	2.41	0.71	1.40	1.85	0.02	$\pi\pi_{\text{NO}_2}^*$
$2^1\text{A}'$	4.13	0.59	4.01	2.31	2.39	2.50	0.10	CT
$3^1\text{A}'$	4.48	0.02	3.08	0.84	2.29	1.99	0.05	CT
$2^1\text{A}''$	4.54	0	2.42	0.66	1.43	1.88	0.03	$\pi\pi_{\text{NO}_2}^*$
$4^1\text{A}'$	5.80	0.01	3.19	0.92	2.42	2.40	0.20	$\pi\pi^*$

state $4^1\text{A}'$ can be identified as a $\pi\pi^*$ transition delocalized over the entire molecule. This is reflected in the large and almost equal hole and electron sizes of about 2.4 Å, and the relatively small amount of CT with $d_{\text{h} \rightarrow \text{e}} = 0.92$ Å. Interestingly, this excited state has a strong electron–hole correlation, a feature which is only revealed by exciton descriptors as $R_{\text{eh}} = 0.195$.

4 Estimating charge-transfer character

Charge transfer or electron transfer, also referred to as exciton fission is an important step in many biophysical and technological processes.^{44–50} Photosynthesis as well as photovoltaic devices are driven by light-induced charge separation, and an in depth understanding of the fundamental charge-transfer processes is crucial for technological progress. Concomitantly, the theoretical investigation and prediction of charge-transfer processes has attracted great interest over the last decades. However, as important charge-transfer states are for technology and biology, as problematic they are to be described by time-dependent density functional theory (TDDFT),^{51–53} which is

**Fig. 3** Hole (blue) and electron (red) densities³⁸ of first five singlet excited states of *para*-nitrodimethylaniline calculated at the ADC(2)/6-311G(d,p) level of theory rendered with VMD.⁴³

de facto the standard method for the description of excited states of large organic molecules and aggregates.¹ Therefore, the description of CT states by TDDFT and the development of diagnostic measure to detect CT states has become a prominent research field and a variety of excited-state descriptors have been designed with the aim to detect charge-transfer states.^{39,54–59}

A first idea was to calculate the orbital overlap Λ as diagnostic tool in order to identify states with charge-transfer character.³⁹ While this so-called Λ -value provides useful information for excited states with spatially separate hole and electron, it is

not suitable to identify states with small degrees of CT or charge-resonance states.⁶⁰ For example in the case of 1L_a and 1L_b states of oligoacenes, the A values have been proven insufficient to explain the discrepancy in accuracy of the two states.^{29,61,62} Although A is as high as 0.9 for the 1L_a (which corresponds to a very high overlap), this state shows a strong dependence of the excitation energy on the fraction of non-local exchange included in the xc-functional, as is typical for the “CT-failure” of TDDFT.

Another popular strategy employed in many descriptors is connected to the fact that charge-transfer states possess a significant dipole moment. But instead of measuring the dipole itself, the idea is to measure the distance between the centroids of the generated positive and negative charges. There are several different quantities which can be examined for this purpose such as the 1TDM, the difference density or one-particle difference density matrix (1DDM), and using relaxed or unrelaxed densities, as well as different mathematical approaches, which have been tested as diagnostic tools for TDDFT. The choice of underlying quantity and mathematical approach directly influence the predictive power of the different descriptors and it can be quite difficult to tell which one is the most relevant or important one to judge the quality of the computational results.

After all, it became apparent that neither the identification of electron-hole overlap, nor a measure of charge separation suffice to reliably identify all problematic cases. To accurately and reliably capture problematic cases such as charge-resonance or excitonic states, the focus has to be shifted from charge transfer to electron-hole correlation. Exactly this line of thought is followed in exciton analysis, where different exciton properties are considered. These are the spatial size of the exciton, the hole-electron distance, but more importantly also electron-hole correlation effects, which are crucial to identify charge-transfer and charge-resonance states unequivocally. Thereby, differences in accuracies of different xc-functionals can nicely be understood and explained.^{26,28,29}

Putting this approach into practice, let us in the following sections take a closer look at a prototypical system featuring charge transfer, α -(NMe₂) ω -(NO₂)(phenylene)_{*n*}.^{58,63,64} In this system, charge transfer between the push and pull groups, *i.e.*, NMe₂ and NO₂ can be studied in an organic molecule. Furthermore, as the number of phenyl linkers increases, charge transfer between the end groups should be less favorable due to the $\frac{1}{r}$ -scaling of the Coulomb attraction between hole and electron. Simultaneously, as the extended π -system grows, delocalized $\pi\pi^*$ excitations are expected to become energetically competitive. Three different xc-functionals are selected, two standard hybrid functionals with a relatively small amount of non-local orbital exchange, B3LYP⁶⁵ (21%) and PBE0^{66,67} (25%), and the long-range corrected functional CAM-B3LYP⁶⁸ (21–65%) which scales the amount of non-local exchange as a function of the interelectron distance. These functionals have been used earlier by Maschietto *et al.*⁶⁴ and Etienne *et al.*⁵⁸ to study the same systems and we will compare our calculated data with the other data sets in the following.

To trace the effects of CT and extended π -delocalization, we focus on the S_1 state of α -(NMe₂) ω -(NO₂)(phenylene)_{*n*} with $n = 1$ –5 (counting the number of phenyl rings) and calculated it at the full-TDDFT/6-311G(d,p) level. While Maschietto *et al.* follow the same strategy and study the S_1 , Etienne *et al.* set a different focus and follow states described by the same NTOs, which leads to a different selection of states for CAM-B3LYP, where only for the system with $n = 5$ the S_1 is investigated.

Excitation energies calculated in this work and in works by Etienne *et al.*⁵⁸ and Maschietto *et al.*⁶⁴ are plotted against the number of phenyl rings n in Fig. 4(a). The most apparent difference is the overall trend in excitation energies when comparing PBE0 and B3LYP to CAM-B3LYP. The excitation energies calculated with B3LYP and PBE0 are ≥ 1 eV smaller for all systems with $n > 1$ than with CAM-B3LYP. While the excitation energies calculated with B3LYP and PBE0 decrease for increasing chain length, they remain almost constant with CAM-B3LYP. This can be traced back to a spurious overstabilization of CT states at the TDDFT/B3LYP and TDDFT/PBE0 levels. To create a platform for further comparison of excited-state descriptors in the following, let us quickly compare the data sets among each other. There are two trends worth noting. While the values for PBE0 and B3LYP agree very well for all three data sets, there are some major differences in the CAM-B3LYP data. In the case of Etienne's data set (dotted lines), this can be explained by the choice of excited states as described above. In Maschietto's data set only the excitation energy of the largest system with $n = 5$ deviates as much as +0.5 eV with CAM-B3LYP.

After this first overview about trends in excitation energies, the next important step is to gain insight into the character of the excited states calculated with different xc-functionals. To quantify the CT character of the S_1 , we will now consider measures for direct charge transfer presented in Fig. 4(b). The black solid line represents the distance between the N atoms of the push and pull groups for each molecule to relate the CT measures to the molecular size. The charge-transfer measures $d_{h \rightarrow e}$, ζ and $^U D_{CT}$ all quantify the charge centroid distance between electron and hole position. Definitions of the latter two descriptors are given in the ESI† and the respective original works.^{54,58,64} In the cases of B3LYP and PBE0, all three descriptors

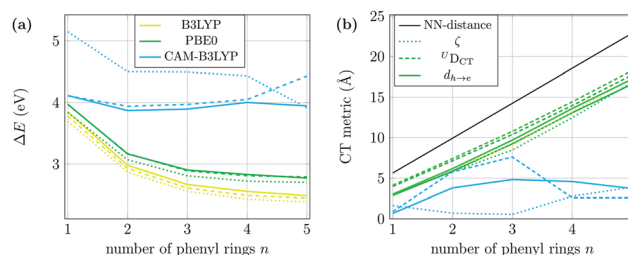


Fig. 4 (a) Excitation energies (ΔE , eV) and (b) CT metrics of (first) singlet excited state of push-pull system α -(NMe₂) ω -(NO₂)(phenylene)_{*n*} calculated at the TDDFT/6-311G(d,p) level of theory in combination with PBE0, B3LYP and CAM-B3LYP xc-functionals: solid lines libwfa; dotted lines Etienne *et al.*⁵⁸ dashed lines Maschietto *et al.*⁶⁴ Color code in (a) also applies to (b).

show the same trend of a linearly increasing charge separation with increasing system size which grows from approximately 4 Å to 17 Å. These trends agree nicely with the observations and conclusions drawn from excitation energies. Taking a closer look at the differences between the CT measures, ζ and $d_{h \rightarrow e}$ are very similar, while $^U D_{CT}$ lies above the two for all systems considered as predicted by Etienne *et al.*⁵⁸ Proceeding to the description of the S_1 at the TDDFT/CAM-B3LYP level, the charge-transfer measures show a significantly different trend for growing system size. First, we will analyze $d_{h \rightarrow e}$. While for the smallest system, *para*-nitrodimethylaniline, the electron–hole separation is smaller than 1 Å, it rises to a value of approximately 5 Å for $n = 3$, after which it slightly decreases again. Hence, a certain spatial separation of electron and hole is observed in the S_1 , however, it does not span the entire molecule and we will postpone further interpretation to the next section. Coming back to the comparison of different CT descriptors, a somewhat similar trend for D_{CT} can be observed. However, especially for the systems with $n = 2, 3$, it seems less obvious that the CT character is reduced at the TDDFT/CAM-B3LYP level as compared to the other xc-functionals. In the case of ζ , the differences to $d_{h \rightarrow e}$ can be traced back to the characterization of different excited states as discussed earlier. However, for the largest system where the same state is analyzed, the values of ζ and $d_{h \rightarrow e}$ are on top of each other. Summarizing the trends in different descriptors, $^U D_{CT}$ appears to be less sensitive than ζ and $d_{h \rightarrow e}$, because the latter two reveal more obviously the change of excitation character of S_1 with CAM-B3LYP.

As a side-aspect, the influence of relaxation effects on the different CT metrics and *vice versa* will be briefly discussed as this can be accessed by calculating D_{CT} from unrelaxed and relaxed densities.⁶⁴ A similar assessment can be provided by $d_{h \rightarrow e}$ when combining it with the 1TDM and the 1DDM, however, only for *ab initio* excited-state methods which account for orbital relaxation. Therefore, we calculated singlet excited states for the systems with $n = 1$ –3 at the ADC(2) level of theory, see Table 4. To rationalize the different effects taken into account in unrelaxed *vs.* relaxed densities, it is helpful to consider a transition between two electronic states as a two-step procedure. Firstly, the initial excitation invokes a change in the electron density. Secondly, the electrons rearrange according to the new configuration, *i.e.*, electron relaxation takes place. Both steps are important to gain insight into the excitation process and experimental findings and one key question will be how to judge the reliability of a computational protocol according to the accessed data.

In the case of a charge-transfer excitation, we expect high values of $d_{h \rightarrow e}$, ζ and $^U D_{CT}$. In the course of density relaxation,

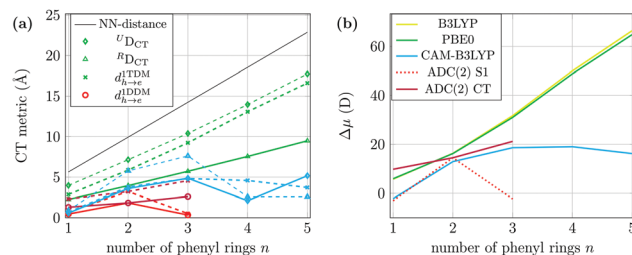


Fig. 5 (a) CT metrics: $^U D_{CT}$ (\diamond , Å, dashed line), $^R D_{CT}$ (Δ , Å, solid line), $d_{h \rightarrow e}^{1TDM}$ (\times , Å, dashed line) and $d_{h \rightarrow e}^{1DDM}$ (\circ , Å, solid line), and (b) difference between excited-state and ground-state dipole moments ($\Delta\mu$, D) of (first) excited state of push–pull system α -(NMe₂) ω -(NO₂)(phenylene) _{n} calculated at the ADC(2) (red) and TDDFT/6-311G(d,p) levels of theory in combination with B3LYP (yellow), PBE0 (green) and CAM-B3LYP (cyan) xc-functionals.

the amount of CT is then reduced as the electrons partially compensate the vertical electron shift. This effect is observed when comparing $^U D_{CT}$ with $^R D_{CT}$ plotted in Fig. 5(a). In this data series, $^U D_{CT} > ^R D_{CT}$ for all states except the S_1 of α -(NMe₂) ω -(NO₂)(phenylene)₅ calculated with CAM-B3LYP. It is furthermore worth noting that the two metrics are almost identical for states with small amount of CT hinting towards very small relaxation effects for these states. For a detailed analysis of relaxation effects calculated using the post-linear response Z-vector method the reader is referred to ref. 69.

In general, the descriptors described so far measure the charge separation distance, and hence, only yield information which could equally well be obtained when the static dipole moments of ground and excited state are compared, see Fig. 5(b). As a consequence, only the most obvious, static characteristics of the electronic structure of the excited states is revealed by these descriptors. The most relevant information to identify failures of TDDFT was simply revealed by comparing xc-functionals with different amount of non-local orbital exchange and their influence on the description of the excited states.²⁹ However, an even more rigorous approach is to consider electron–hole correlation as the primary quantity underlying the shortcomings of TDDFT. This opens a path to identify the most reliable xc-functionals not only with respect to excitation energies, but moreover also with respect to the electronic structure of any excited state, leading eventually to a correct description of photochemistry and photophysics.

In an attempt to offer a general solution to the functional dependence of TDDFT, Kuritz *et al.*⁶² have shown that optimally tuned xc-functionals can recover predictive power for excitation energies in cases where other conventional xc-functionals fail. A future task of exciton analysis is to check whether the good description of excitation energies also coincides with a quantitatively correct description of excited-state electronic structure and properties compared to *ab initio* data.

5 A closer look at electron–hole correlation

So far, we have seen different xc-functionals to describe excited states qualitatively differently as has been revealed by the

Table 4 Collected *ab initio* reference data of (first) excited states of the push–pull system α -(NMe₂) ω -(NO₂)(phenylene) _{n} calculated at the ADC(2) level of theory. 6-311G(d,p) basis for **1** and **2**, 6-31G(d,p) basis for **3**

n /state	ΔE (eV)	f_{osc}	$\Delta\mu$	d_{exc}	$d_{h \rightarrow e}^{1TDM}$	$d_{h \rightarrow e}^{1DDM}$
1/ S_1	3.892	0	−3.04	2.41	0.71	0.46
1/ S_2	4.131	0.591	9.77	4.01	2.31	1.30
2/ S_1	3.782	0.634	14.48	5.30	3.23	1.83
3/ S_1	3.913	0.042	−2.29	2.76	0.52	0.34
3/ S_2	3.987	1.012	21.19	6.70	4.56	2.60

CT measures. To gain a better understanding of how these differences arise, it is interesting to further explore the excited states and in particular to examine electron–hole correlation. As pointed out in the introduction, the generated hole and excited electron interact with each other resulting in different structures of wavefunctions and densities. The main driving forces are the Coulomb attraction between the two oppositely charged quasiparticles and the exchange repulsion. In this section, a visualization technique and excited-state descriptors are presented which provide information about electron–hole correlation.

First, we will examine excited states of the push–pull compounds α -(NMe₂) ω -(NO₂)(phenylene)_n in terms of so-called electron–hole correlation plots.^{14,38,71} These plots are designed to illustrate the interdependence of electron and hole positions in a molecular system, *i.e.*, from where to where electron density is promoted during the excitation. To generate these plots, the molecules are split into functional groups as displayed in Fig. 6(a) for the trimer. The shift in one-electron density is represented by a pseudo-color plot, where the intensity for

electron transition between two fragments is marked in grey scale. For the smallest molecule, *para*-nitrodimethylaniline, there are three functional groups: the nitro group (NO₂), the phenyl ring, and the dimethylamino group (NMe₂). Local excitations at each group are displayed on the main diagonal (going from lower left to upper right), while charge transfer between different groups appears as off-diagonal contributions. The hole (electron) distribution is displayed along the *x*-axis (*y*-axis). For a detailed description of how these plots are composed, please be referred to Fig. S2 in the ESI.† In the case of B3LYP, almost 70% of the excited state is characterized by a shift of electron density from NMe₂ and the phenyl group towards NO₂. A smaller fraction of about 20% is shifted locally within the phenyl ring, and another 15% is shifted from the dimethylamino group towards the phenyl ring. In the case of CAM-B3LYP, the first excited state S₁ is a local excitation of the nitro group. The S₂ at the CAM-B3LYP/TDDFT level, in contrast, is very similar to the S₁ for B3LYP and PBE0, *cf.* Fig. 6(b) first row.

Proceeding to larger push–pull compounds (*n* = 2–5), the S₁ as described by B3LYP and PBE0 possesses prototypical CT character, where the charge is promoted from the NMe₂ group as well as the neighboring phenyl ring towards the other end of the molecule. Both, the outmost phenyl ring attached to NO₂ and NO₂ itself are acting as main electron acceptors. Large parts of the aromatic linker do not take part in the excitation process as illustrated by the almost white diagonal elements. In the case of CAM-B3LYP, the appearance of the electron–hole correlation plots significantly differs. While a clear direction of electron transfer towards NO₂ is observed, the local excitation character of the phenylene linkers becomes predominant, a trend that becomes more pronounced for larger systems. For the largest system with *n* = 5, the first excited state at the CAM-B3LYP level has only a very reduced CT character. Instead, it has predominant contributions on the main diagonal and CT mainly between neighboring functional groups. In earlier works,^{26,72} these states have been identified as Wannier excitons characterized by a certain, finite electron–hole separation. While for the same system (last two rows in Fig. 6), the S₁ at the B3LYP and PBE0 levels is clearly the same prototypical CT state as for the smaller systems, the second excited state, S₂, is more delocalized, which is more pronounced using PBE0 than B3LYP. To provide a theoretical perspective on these results, one can interpret this as a gradual onset of Coulomb binding between electron and hole as the fraction of non-local orbital exchange in the xc-functional increases. For a more detailed discussion of exciton formation and its dependence on the functional choice, the reader is referred to ref. 26.

A quantitative analysis of the S₁ state in terms of exciton sizes and electron–hole correlation coefficients is presented in Fig. 7. The trends in exciton size are compared to the distance between the N-atoms of both functional groups, NMe₂ and NO₂, to provide a comparison to the molecular size. For B3LYP and PBE0, exciton sizes increase linearly with the length of the molecule, however, the slope is less steep than the growth in N–N distance. For CAM-B3LYP, the exciton size follows the trends of the former xc-functionals for *n* = 1, 2, but after that quickly levels

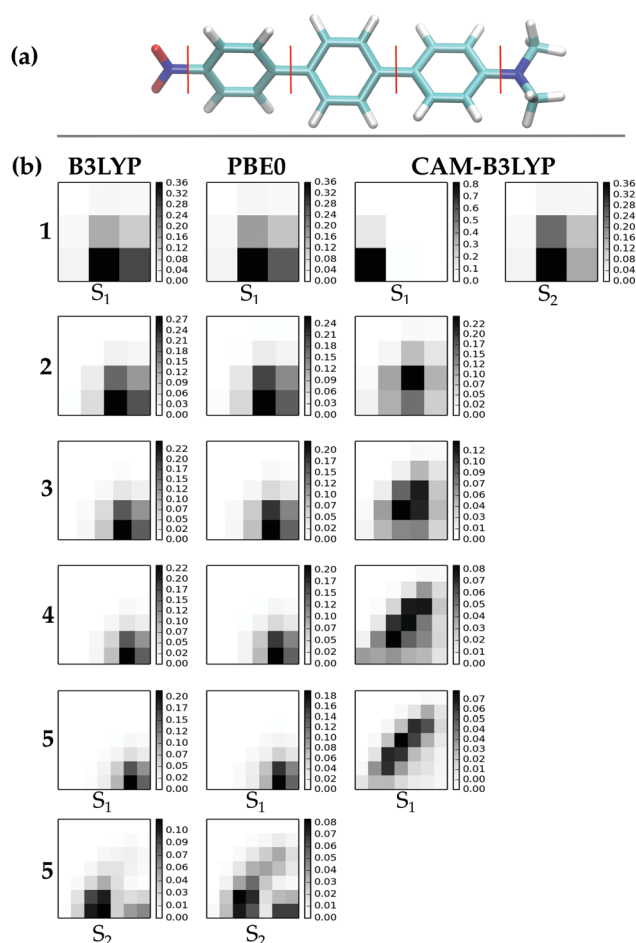


Fig. 6 (a) Fragmentation scheme, (b) electron–hole correlation plots of S₁ if not specified for α -(NMe₂) ω -(NO₂)phenylenes with *n* = 1–5 linkers calculated at the TDDFT/6-311G(d,p) level in combination with B3LYP, PBE0 and CAM-B3LYP xc-functionals. Plots generated with TheoDRE.⁷⁰ Note the individual scale for each plot.

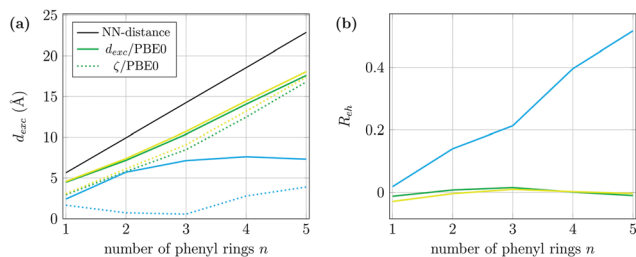


Fig. 7 (a) Exciton sizes (d_{exc} , Å) and (b) correlation coefficients (R_{eh}) of first singlet excited state of push-pull system α -(NMe₂) ω -(NO₂)(phenylene)_n calculated at the TDDFT/6-311G(d,p) level of theory in combination with B3LYP (yellow), PBE0 (green), and CAM-B3LYP (cyan) xc-functionals.

off and converges against a value of approx. 7.3 Å. This trend has been previously observed for a variety of different conjugated π -systems for long-range corrected xc-functionals and *ab initio* calculations and can be interpreted as exciton formation.²⁶ Electron-hole correlation coefficients R_{eh} provide an explanation for the observed trends. While the CT state as described by B3LYP and PBE0 shows no electron-hole correlation and R_{eh} is essentially zero, the exciton formation as observed with CAM-B3LYP is accompanied by an almost linear increase in R_{eh} from 0 to 0.45.

Electron-hole correlation effects do play an important role for a characterization of excited states. Their visualization and quantification provides a description of the electronic structure and an in-depth understanding of excited states in much more detail as compared to the previous static charge-transfer measures. This allows for straightforward analyses and investigation of phenomena like exciton formation and fission, as well as charge resonance with quantum-chemical calculations, a task which is still considered particularly challenging. An accurate theoretical description of electron-hole correlations by quantum-chemical methods is furthermore crucial for a physically correct description of molecular photochemistry. Due to the quantitative, and easy-to-use nature of the exciton descriptors, they allow for systematic benchmarking of quantum-chemical methods taking not only the energy but also complex properties of the electronic structure into account, which will be the topic of the next section.

6 Benchmarking excited-state methods with exciton properties

Benchmarking is an every-day task in quantum chemistry.^{3,73–82} It has the aim to bridge the gap between highly accurate *ab initio* calculations, which are limited to systems of small to medium sizes due to their high computational demands, and approximate, yet computationally efficient methods, which are thus applicable to large size systems. To ensure sufficient accuracy of the results obtained by the latter methods, their computational results need to be compared to high-level theoretical benchmark or experimental data. A central and obviously important criterion for excited-state methods are the computed excitation energies. However, these scalar quantities do not necessarily reflect the general quality of the theoretical description

of a complex molecular system, as high accuracy of an energy can always be, and often is, obtained by fortuitous cancellation of errors.

Exciton properties offer a quantitative description of the complex excited-state electronic structure based on the transition density alone without reference to a particular electronic structure method. Since they can thus be employed with any excited-state method, exciton descriptors provide a new set of criteria for comparing results of different excited-state methods quantitatively and are excellent means for benchmarking.²⁸ Benchmarking with respect to excitation energies alone has been shown previously, in selected cases, to be in favour of a theoretical methodology which does not provide a physically correct description of the electronic structure of the excited states.²⁸

As pedagogical example, a benchmark study of the first three singlet excited states of *para*-nitrodimethylaniline, which have already been discussed in Section 3, is presented. The selected states have been calculated at the ADC(3)/6-311G(d,p) and EOM-CCSD/6-311G(d,p) levels of theory and compared to the previously presented ADC(2) and TDDFT data. While the complete data set is available in the ESI,[†] here the focus is on some key properties for benchmarking shown in Fig. 8.

Inspecting first the excitation energies in Fig. 8(a), the state ordering is preserved by all methods except by TDDFT when the B3LYP and PBE0 xc-functionals are employed, in which the S_1 and S_2 are interchanged. For the sake of comparability, they have been sorted such that they are in line with the rest of the data set, *i.e.*, S_1 at B3LYP and PBE0 level are presented along with $2^1A'$ and the respective S_2 along with the $1^1A''$ state. Compared to ADC(3), the excitation energies obtained at the EOM-CCSD level are generally higher, while they are smaller at the ADC(2) level. Among the TDDFT values with different xc-functionals, there is a clear trend towards increasing excitation

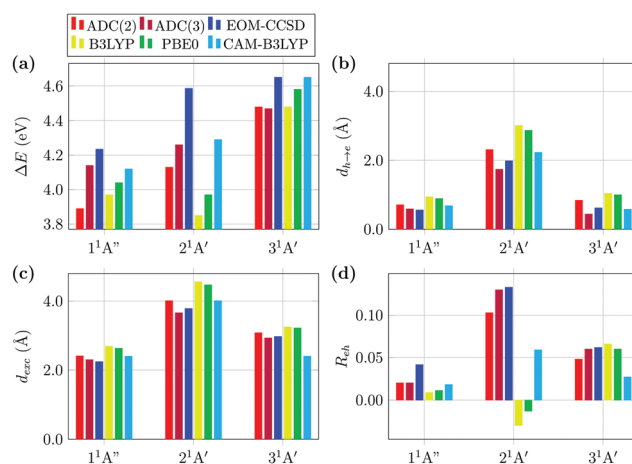


Fig. 8 (a) Excitation energies (ΔE , eV), (b) charge centroid separation ($d_{h \rightarrow e}$, Å), (c) exciton size (d_{exc} , Å) and (d) electron-hole correlation coefficient (R_{eh}) of first three singlet excited states computed at the ADC(3), ADC(2) and EOM-CCSD and TDDFT levels of theory, the latter in combination with B3LYP, PBE0 and CAM-B3LYP xc-functionals, employing the 6-311G(d,p) basis set. Legend in (a) applies to all plots in this figure.

energies when going from B3LYP to PBE0 and CAM-B3LYP, which is a typical result of an increasing amount of non-local orbital exchange. Since the excitation energies of the *ab initio* methods are somewhat spread, it remains to the taste of the observer to judge which xc-functional is the most accurate. The state ordering might be a decisive factor to choose CAM-B3LYP rather than one of the other functionals in this case. Considering the root-mean-square (rms) deviations, however, PBE0 shows the best performance compared to ADC(2) with a variation of 0.14 eV, and CAM-B3LYP performs worst with 0.19 eV. On the contrary using ADC(3) and EOM-CCSD as reference, CAM-B3LYP performs best with rms deviations of 0.10 eV and 0.18 eV, respectively. Conclusions drawn from such benchmarking can thus greatly vary.

Taking a look at static exciton properties, a clear distinction of the electronic structure of the $2^1A'$ state, which shows a significant separation of electron and hole charge centroids, from the other two states can be recognized (Fig. 8(b)). At the same time, the electron-hole distance strongly depends on the employed method and $d_{h \rightarrow e}$ is almost 1 Å larger for B3LYP and PBE0 than for the other methods. This provides an explanation for the observed state switching of S_1 and S_2 at TDDFT/B3LYP and TDDFT/PBE0 levels, which is associated with the CT failure of TDDFT artificially lowering excitation energies of CT states. Concerning the *ab initio* methods, ADC(2) yields slightly more pronounced CT character of the $2^1A'$ state than ADC(3) and EOM-CCSD, while the latter two stand in nice agreement with each other.

Exciton sizes (Fig. 8(c)) take into account different, competing effects. The trends in charge separation as discussed before are also observed, but in addition slight modulations in electron-hole correlation as well as in hole and electron sizes are considered as well, see eqn (12). This is particularly evident from inspecting the $3^1A'$ state. While the static charge separation as described by $d_{h \rightarrow e}$ of the CAM-B3LYP result is similar to the *ab initio* references, a significantly smaller exciton size is found. Taking a look at electron-hole correlation, the comparably small correlation coefficient is, however, not small enough to fully explain the discrepancy. Exploring this issue further and taking a look at electron and hole size (see ESI†), it becomes clear that the S_3 at the CAM-B3LYP level corresponds indeed to the S_4 ($2^1A''$) state at the ADC(2) level and possesses local $n\pi^*$ character. Finding such discrepancies in large data sets using standard density or orbital visualization techniques can be rather tedious, maybe impossible. Hence, this case nicely illustrates the benefits of the quantitative exciton analysis.

As final and particularly insightful exciton descriptor, correlation coefficients R_{eh} are presented in Fig. 8(d). The most remarkable observation is the large discrepancy between *ab initio* methods and TDDFT methods in describing electron-hole correlation of the $2^1A'$ state. While the values of R_{eh} at EOM-CCSD, ADC(2) and ADC(3) levels are well above 0.1, it is only about half the size at TDDFT/CAM-B3LYP level (0.06) and even negative at TDDFT/B3LYP and TDDFT/PBE0 levels (−0.03 and −0.01). In other words, while hole and electron attract each

other at EOM-CCSD, ADC(2), ADC(3) and TDDFT/CAM-B3LYP levels and thus correlated, at TDDFT/B3LYP and TDDFT/PBE0 levels they avoid each other and are thus anti-correlated. This trend is particularly interesting as it provides the reason for the poor performance of B3LYP and PBE0 in the case of this partial CT state. Not only is the CT character overpronounced, but also electron-hole Coulomb attraction as found in the *ab initio* results is not properly described by these xc-functionals. Coulomb-type electron-hole attraction in the linear response formalism of TDDFT originates from non-local Hartree-Fock exchange. Hence only a small fraction of 21% and 25% of it is considered in B3LYP and PBE0, respectively. As a consequence, electron-hole exchange repulsion falsely overweights electron-hole Coulomb attraction when xc-functionals with low amounts of non-local Hartree-Fock exchange are employed.

Concluding the results of this section, exciton analysis revealed that CAM-B3LYP (as the only long-range corrected functional included in this small pedagogical study) provides the most accurate description of the electronic structure of the evaluated states as compared to all *ab initio* data. It is particularly interesting to note that all *ab initio* methods describe all three states very similar in terms of exciton properties despite discrepancies in excitation energies. Going beyond the presented example, it is worth realizing that only a small selected set of exciton descriptors has been employed here which quantifies the most relevant properties for the excited states. However, already this small pedagogical example demonstrates the usefulness and strengths of this novel approach to evaluate excited-state methods. For a comprehensive overview how to evaluate the accuracy for different types of excited states provided by different excited-state quantum-chemical methods exploiting exciton properties, e.g. for Rydberg, CT, excitonic or doubly excited states, the reader is referred to ref. 28.

7 Summary and conclusions

Very often the electronic structure of excited electronic states is analyzed by visually inspecting the molecular orbitals involved in the electronic transition. However, this is generally not sufficient, when several orbital transition are involved or multiple electrons are excited. More suitable and generally applicable approaches to analyze the electronic structure of excited states and to identify the character of an electronic transition are based on the visualization of the one-electron transition density or the one-electron difference density and/or the corresponding natural transition orbitals or natural difference orbitals. Nevertheless, visual inspection always relies on the perception of the observer and her/his interpretation and is difficult to automate.

In this perspective, we focused on the description of novel exciton descriptors, which are quantum mechanically computed expectation values of an exciton wavefunction derived from the transition density matrix. They offer the great advantage of a clear physical concept underlying the interpretation of the individual descriptors and give access to a variety of

excited-state properties, some of which have been difficult or impossible to trace so far. It is straightforward to compute hole and electron sizes, the exciton size, hole-electron separation and thereby to quantify charge-transfer character. Perhaps the most useful quantities describe electron-hole correlation allowing to analyze whether electron and hole move in a correlated or anti-correlated manner, which is directly related to whether electron hole move together and attract each other or whether they avoid and repel each other. The combination of exciton descriptors allows in a unique way to gain insight into important fundamental excited-state processes like charge transfer or exciton fission, electron or charge-transfer and charge-resonance effects.

Since exciton descriptors are quantitative, exciton analysis can be automatized, and in addition only a one-electron transition density matrix is needed which is provided by every excited-state method. This offers a unique pathway to benchmarking excited-state methods, because directly comparable data can be obtained for the electronic structure of computed excited states at different levels of theory. Exploiting exciton analysis for benchmarking allows for the evaluation of the applicability of excited-state methods not only with respect to the energy but also with respect to the quality of the electronic structure computed. They thus allow for an automatized multi-parameter benchmarking and evaluation of the quality of a calculation, which is generally useful to be applied in machine learning approaches.

8 Computational details

All calculations were performed using Q-Chem 5.^{83,84} Geometries were optimized at the DFT/PBE0/6-311(d,p) level of theory. All structures are given in the ESI.† Note that despite we used the same methodology as ref. 58 to obtain geometries (PBE0/6-311(d,p)), the structures are more similar to the ones in ref. 64. Excited-state calculations were performed using the standard versions of ADC(2), ADC(3) and EOM-CCSD (no RI) in combination with Pople's 6-311G(d,p) basis set, and in one specified case with Pople's 6-31G(d,p) basis set.⁴⁰ Symmetry labels correspond to Q-Chem standard output. TDDFT calculations (full TDDFT) were performed using B3LYP, PBE0 and CAM-B3LYP xc-functionals in combination with Pople's 6-311G(d,p) basis set.

Conflicts of interest

There are no conflicts to declare.

Acknowledgements

We would like to thank Dr Felix Plasser for his continuous collaboration on the topic of excited-state analysis over the past years. We would like to thank Prof. Anna I. Krylov for discussion on benchmarking with exciton properties. SAM would like to thank Prof. Peter Schwerdtfeger for mentoring. We would like to thank Dr Jan-M. Mewes for proof-reading the manuscript.

Notes and references

- 1 A. Dreuw and M. Head-Gordon, *Chem. Rev.*, 2005, **105**, 4009–4037.
- 2 L. González, D. Escudero and L. Serrano-Andrés, *ChemPhysChem*, 2011, **13**, 28–51.
- 3 A. Dreuw, *ChemPhysChem*, 2006, **7**, 2259–2274.
- 4 I. Fleming, *Molecular Orbitals and Organic Chemical Reactions*, John Wiley & Sons, Ltd, student edition, 2009.
- 5 K. Sneskov and O. Christiansen, *WIREs Comput. Mol. Sci.*, 2012, **2**, 566–584.
- 6 R. Bartlett, *WIREs Comput. Mol. Sci.*, 2012, **2**, 126–138.
- 7 A. I. Krylov, *Annu. Rev. Phys. Chem.*, 2008, **59**, 433–462.
- 8 H. Sekino and R. J. Bartlett, *Int. J. Quantum Chem.*, 1984, **26**, 255–265.
- 9 J. Stanton and R. Bartlett, *J. Chem. Phys.*, 1993, **98**, 7029–7039.
- 10 J. Schirmer, *Phys. Rev. A: At., Mol., Opt. Phys.*, 1982, **26**, 2395–2416.
- 11 A. B. Trofimov and J. Schirmer, *J. Phys. B: At., Mol. Opt. Phys.*, 1995, **28**, 2299–2324.
- 12 A. Dreuw and M. Wormit, *WIREs Comput. Mol. Sci.*, 2015, **5**, 82–95.
- 13 A. V. Luzanov, A. A. Sukhorukov and V. É. Umanskii, *Theor. Exp. Chem.*, 1976, **10**, 354–361.
- 14 A. V. Luzanov and O. A. Zhikol, *Int. J. Quantum Chem.*, 2010, **110**, 902–924.
- 15 A. V. Luzanov and O. V. Prezhdo, *Int. J. Quantum Chem.*, 2005, **102**, 582–601.
- 16 H. S. Yu, S. L. Li and D. G. Truhlar, *J. Chem. Phys.*, 2016, **145**, 130901.
- 17 N. T. Maitra, *J. Chem. Phys.*, 2016, **144**, 220901.
- 18 N. Kirova, *Polym. Int.*, 2008, **57**, 678–688.
- 19 W. Barford and N. Paiboonvorachet, *J. Chem. Phys.*, 2008, **129**, 164716.
- 20 W. Barford, *J. Phys. Chem. A*, 2013, **117**, 2665–2671.
- 21 J. Frenkel, *Phys. Rev.*, 1931, **37**, 17–44.
- 22 S. Brazovskii and N. Kirova, *Chem. Soc. Rev.*, 2010, **39**, 2453–2465.
- 23 S. A. B  ppler, F. Plasser, M. Wormit and A. Dreuw, *Phys. Rev. A: At., Mol., Opt. Phys.*, 2014, **90**, 052521.
- 24 F. Plasser, B. Thomitzni, S. A. B  ppler, J. Wenzel, D. R. Rehn, M. Wormit and A. Dreuw, *J. Comput. Chem.*, 2015, **36**, 1609–1620.
- 25 R. Richard and J. Herbert, *J. Chem. Theory Comput.*, 2011, **7**, 1296–1306.
- 26 S. A. Mewes, F. Plasser and A. Dreuw, *J. Phys. Chem. Lett.*, 2017, **8**, 1205–1210.
- 27 J. Wenzel and A. Dreuw, *J. Chem. Theory Comput.*, 2016, **12**, 1314–1330.
- 28 S. A. Mewes, F. Plasser, A. I. Krylov and A. Dreuw, *J. Chem. Theory Comput.*, 2018, **14**, 710–725.
- 29 S. A. Mewes, F. Plasser and A. Dreuw, *J. Chem. Phys.*, 2015, **143**, 171101.
- 30 D. Hirose, Y. Noguchi and O. Sugino, *J. Chem. Phys.*, 2017, **146**, 044303.
- 31 F. Plasser, S. A. Mewes, A. Dreuw and L. González, *J. Chem. Theory Comput.*, 2017, **13**, 5343–5353.

- 32 R. L. Martin, *J. Chem. Phys.*, 2003, **118**, 4775–4777.
- 33 I. Mayer, *Chem. Phys. Lett.*, 2007, **437**, 284–286.
- 34 M. Head-Gordon, A. M. Graña, D. Maurice and C. A. White, *J. Phys. Chem.*, 1995, **99**, 14261–14270.
- 35 K. Nanda and A. I. Krylov, *J. Phys. Chem. Lett.*, 2017, **8**, 3256–3265.
- 36 W. Skomorowski and A. I. Krylov, *J. Phys. Chem. Lett.*, 2018, **9**, 4101–4108.
- 37 F. Plasser and H. Lischka, *J. Chem. Theory Comput.*, 2012, **8**, 2777–2789.
- 38 F. Plasser, M. Wormit and A. Dreuw, *J. Chem. Phys.*, 2014, **141**, 024106.
- 39 M. J. G. Peach, P. Benfield, T. Helgaker and D. J. Tozer, *J. Chem. Phys.*, 2008, **128**, 044118.
- 40 R. Krishnan, J. S. Binkley, R. Seeger and J. A. Pople, *J. Chem. Phys.*, 1980, **72**, 650–654.
- 41 J.-M. Mewes, Z.-Q. You, M. Wormit, T. Kriesche, J. M. Herbert and A. Dreuw, *J. Phys. Chem. A*, 2015, **119**, 5446–5464.
- 42 J.-M. Mewes, V. Jovanović, C. M. Marian and A. Dreuw, *Phys. Chem. Chem. Phys.*, 2014, **16**, 12393–12406.
- 43 W. Humphrey, A. Dalke and K. Schulten, *J. Mol. Graphics*, 1996, **14**, 33–38.
- 44 T. M. Clarke and J. R. Durrant, *Chem. Rev.*, 2010, **110**, 6736–6767.
- 45 S. Faraji and A. Dreuw, *Photochem. Photobiol.*, 2016, **93**, 37–50.
- 46 M. B. Smith and J. Michl, *Chem. Rev.*, 2010, **110**, 6891–6936.
- 47 M. B. Smith and J. Michl, *Annu. Rev. Phys. Chem.*, 2013, **64**, 361–386.
- 48 D. Casanova, *Chem. Rev.*, 2018, **118**, 7164–7207.
- 49 H. Tamura and I. Burghardt, *J. Am. Chem. Soc.*, 2013, **135**, 16364–16367.
- 50 J. Wenzel, A. Dreuw and I. Burghardt, *Phys. Chem. Chem. Phys.*, 2013, **15**, 11704–11716.
- 51 A. Dreuw and M. Head-Gordon, *J. Am. Chem. Soc.*, 2004, **126**, 4007–4016.
- 52 A. Dreuw, J. L. Weisman and M. Head-Gordon, *J. Chem. Phys.*, 2003, **119**, 2943.
- 53 W. Hieringer and A. Görling, *Chem. Phys. Lett.*, 2006, **419**, 557–562.
- 54 T. Le Bahers, C. Adamo and I. Ciofini, *J. Chem. Theory Comput.*, 2011, **7**, 2498–2506.
- 55 D. Jacquemin, T. Le Bahers, C. Adamo and I. Ciofini, *Phys. Chem. Chem. Phys.*, 2012, **14**, 5383–5388.
- 56 C. A. Guido, P. Cortona, B. Mennucci and C. Adamo, *J. Chem. Theory Comput.*, 2013, **9**, 3118–3126.
- 57 C. A. Guido, P. Cortona and C. Adamo, *J. Chem. Phys.*, 2014, **140**, 104101.
- 58 T. Etienne, X. Assfeld and A. Monari, *J. Chem. Theory Comput.*, 2014, **10**, 3906–3914.
- 59 E. Ronca, M. Pastore, L. Belpassi, F. D. Angelis, C. Angeli, R. Cimирaglia and F. Tarantelli, *J. Chem. Phys.*, 2014, **140**, 054110.
- 60 B. Moore, H. Sun, N. Govind, K. Kowalski and J. Autschbach, *J. Chem. Theory Comput.*, 2015, **11**, 3305–3320.
- 61 Y.-L. Wang and G.-S. Wu, *Int. J. Quantum Chem.*, 2008, **108**, 430–439.
- 62 N. Kuritz, T. Stein, R. Baer and L. Kronik, *J. Chem. Theory Comput.*, 2011, **7**, 2408–2415.
- 63 I. Ciofini, T. Le Bahers, C. Adamo, F. Odobel and D. Jacquemin, *J. Phys. Chem. C*, 2012, **116**, 11946–11955.
- 64 F. Maschietto, M. Campetella, M. J. Frisch, G. Scalmani, C. Adamo and I. Ciofini, *J. Comput. Chem.*, 2018, **39**, 735–742.
- 65 A. D. Becke, *J. Chem. Phys.*, 1993, **98**, 5648–5652.
- 66 C. Adamo and V. Barone, *J. Chem. Phys.*, 1999, **110**, 6158–6170.
- 67 C. Adamo, G. E. Scuseria and V. Barone, *J. Chem. Phys.*, 1999, **111**, 2889–2899.
- 68 T. Yanai, D. P. Tew and N. C. Handy, *Chem. Phys. Lett.*, 2004, **393**, 51–57.
- 69 M. Pastore, X. Assfeld, E. Mosconi, A. Monari and T. Etienne, *J. Chem. Phys.*, 2017, **147**, 024108.
- 70 F. Plasser, TheoDORE: a package for theoretical density, orbital relaxation, and exciton analysis, available from <http://theodore-qc.sourceforge.net/>.
- 71 S. Tretiak and S. Mukamel, *Chem. Rev.*, 2002, **102**, 3171–3212.
- 72 S. A. Mewes, J.-M. Mewes, A. Dreuw and F. Plasser, *Phys. Chem. Chem. Phys.*, 2016, **18**, 2548–2563.
- 73 H. Koch, O. Christiansen, P. Jørgensen and J. Olsen, *Chem. Phys. Lett.*, 1995, **244**, 75–82.
- 74 M. Schreiber, M. R. Silva-Junior, S. P. A. Sauer and W. Thiel, *J. Chem. Phys.*, 2008, **128**, 134110.
- 75 D. Jacquemin, V. Wathelot, E. A. Perpète and C. Adamo, *J. Chem. Theory Comput.*, 2009, **5**, 2420–2435.
- 76 A. D. Laurent and D. Jacquemin, *Int. J. Quantum Chem.*, 2013, **113**, 2019–2039.
- 77 R. Send, M. Kühn and F. Furche, *J. Chem. Theory Comput.*, 2011, **7**, 2376–2386.
- 78 D. Kánnár and P. G. Szalay, *J. Chem. Theory Comput.*, 2014, **10**, 3757–3765.
- 79 D. Jacquemin, B. Mennucci and C. Adamo, *Phys. Chem. Chem. Phys.*, 2011, **13**, 16987–16998.
- 80 S. Knippenberg, R. L. Gieseck, D. R. Rehn, S. Mukhopadhyay, A. Dreuw and J.-L. Brédas, *J. Chem. Theory Comput.*, 2016, **12**, 5465–5476.
- 81 E. Brémond, M. Savarese, A. J. Pérez-Jiménez, J. C. Sancho-García and C. Adamo, *J. Chem. Theory Comput.*, 2017, **13**, 5539–5551.
- 82 M. Pastore, E. Mosconi, F. De Angelis and M. Grätzel, *J. Phys. Chem. C*, 2010, **114**, 7205–7212.
- 83 A. I. Krylov and P. M. W. Gill, *WIREs Comput. Mol. Sci.*, 2013, **3**, 317–326.
- 84 Y. Shao, Z. Gan, E. Epifanovsky, A. T. Gilbert, M. Wormit, J. Kussmann, A. W. Lange, A. Behn, J. Deng, X. Feng, D. Ghosh, M. Goldey, P. R. Horn, L. D. Jacobson, I. Kaliman, R. Z. Khaliullin, T. Kuś, A. Landau, J. Liu, E. I. Proynov, Y. M. Rhee, R. M. Richard, M. A. Rohrdanz, R. P. Steele, E. J. Sundstrom, H. L. Woodcock III, P. M. Zimmerman, D. Zuev, B. Albrecht, E. Alguire, B. Austin, G. J. O. Beran, Y. A. Bernard, E. Berquist, K. Brandhorst, K. B. Bravaya, S. T. Brown, D. Casanova,

C.-M. Chang, Y. Chen, S. H. Chien, K. D. Closser, D. L. Crittenden, M. Diedenhofen, R. A. DiStasio Jr., H. Do, A. D. Dutoi, R. G. Edgar, S. Fatehi, L. Fusti-Molnar, A. Ghysels, A. Golubeva-Zadorozhnaya, J. Gomes, M. W. Hanson-Heine, P. H. Harbach, A. W. Hauser, E. G. Hohenstein, Z. C. Holden, T.-C. Jagau, H. Ji, B. Kaduk, K. Khistyayev, J. Kim, J. Kim, R. A. King, P. Klunzinger, D. Kosenkov, T. Kowalczyk, C. M. Krauter, K. U. Lao, A. D. Laurent, K. V. Lawler, S. V. Levchenko, C. Y. Lin, F. Liu, E. Livshits, R. C. Lochan, A. Luenser, P. Manohar, S. F. Manzer, S.-P. Mao, N. Mardirossian, A. V. Marenich, S. A. Maurer, N. J. Mayhall, E. Neuscamman, C. M. Oana, R. Olivares-Amaya, D. P. O'Neill, J. A. Parkhill, T. M. Perrine, R. Peverati, A. Prociuk, D. R. Rehn, E. Rosta, N. J. Russ,

S. M. Sharada, S. Sharma, D. W. Small, A. Sodt, T. Stein, D. Stück, Y.-C. Su, A. J. Thom, T. Tsuchimochi, V. Vanovschi, L. Vogt, O. Vydrov, T. Wang, M. A. Watson, J. Wenzel, A. White, C. F. Williams, J. Yang, S. Yeganeh, S. R. Yost, Z.-Q. You, I. Y. Zhang, X. Zhang, Y. Zhao, B. R. Brooks, G. K. Chan, D. M. Chipman, C. J. Cramer, W. A. Goddard III, M. S. Gordon, W. J. Hehre, A. Klamt, H. F. Schaefer III, M. W. Schmidt, C. D. Sherrill, D. G. Truhlar, A. Warshel, X. Xu, A. Aspuru-Guzik, R. Baer, A. T. Bell, N. A. Besley, J.-D. Chai, A. Dreuw, B. D. Dunietz, T. R. Furlani, S. R. Gwaltney, C.-P. Hsu, Y. Jung, J. Kong, D. S. Lambrecht, W. Liang, C. Ochsenfeld, V. A. Rassolov, L. V. Slipchenko, J. E. Subotnik, T. V. Voorhis, J. M. Herbert, A. I. Krylov, P. M. Gill and M. Head-Gordon, *Mol. Phys.*, 2015, **113**, 184–215.